JST: Engineering and Technology for Sustainable Development
Volume 32, Issue 1, March 2022, 030-037

Thermodynamic Properties of Potential Alternative Refrigerant HFO-1234ze(Z)

Phan Thi Thu Huong[1], Lai Ngoc Anh[2,*], Nguyen Nguyen An[2], Ta Van Chuong[2]
[1]Nam Dinh University of Technology Education, Nam Dinh, Vietnam
[2]Hanoi University of Science and Technology, Hanoi, Vietnam
[*]Email: anh.laingoc@hust.edu.vn

Abstract

Cis-1,3,3,3-Tetrafluoropropene HFO-1234ze(Z) is an environmentally friendly potential alternative refrigerant for heat-pump application. In usability evaluation of this refrigerant in heat pump application, the accurate thermodynamic properties of HFO-1234ze(Z) in both single-phase and two-phase regions are needed. So, this paper aims to provide an accurate lgP-h diagram and the thermodynamic properties in both single-phase and two-phase regions. The accuracy of this published data and the lgP-h diagram was evaluated by comparing this data with available experimental data. The study shows that the average absolute deviations between our values and experimental data for vapour pressure, saturated liquid density, subcooled liquid density and gaseous pressure are 0,34%, 0,42%, 0,60%, and 0,99%, respectively. Additional evaluations for the ideal gas heat capacities and speed of sound are available in this work. The average absolute deviations between calculated values and published data for compressed liquid speed of sound, gaseous speed-of-sound data, and ideal gas heat capacity are 2.2%, 0,98%, 0,57%, respectively.

Keywords: Cis-1,3,3,3-Tetrafluoropropene HFO-1234ze(Z), lgP-h diagram R1234ze(Z), thermodynamic data, saturated vapour and liquid table, subcooled liquid and superheated table.

1. Introduction

Due to the ozone-depleting and the global warming problems, the Montreal Protocol [1] and the Kyoto protocol were proposed and implemented to reduce the greenhouse gas emissions such as chlorofluorocarbon (CFC) and hydrochlorofluorocarbon (HCFC), and hydrofluorocarbons HFCs [2]. In the past decades, R245fa was considered as the alternative refrigerant for R114 in the medium and high temperature heat pump. R245a has a 100-year Global Warming Potential (GWP) of 659 [3]. Many countries have issued policies and regulations to reduce or eliminate the use of R245fa such as the US significant new alternatives policy (SNAP) [4], EU F-gas regulation [5], Japan revised F-gas regulation [6]. Thus, the study on new potential environmentally friendly substances is interesting and meaningful.

HFO-1234ze(Z) has been proposed as the potential alternative refrigerant and working fluid as HFO-1234ze(Z) has the ozone depletion potential (ODP) of 0, lower flammability limit of 0.211, and GWP100 = 1.4 [7]. The HFO-1234ze(Z) is classified as mildly flammable, non-toxic (A2L). To confirm whether this refrigerant is suitable substitute, the accurate thermodynamic properties of HFO-1234ze(Z) in both single-phase and two-phase regions are necessary. Only a few studies on the thermodynamic properties of HFO-1234ze(E) have been done and published [8-12]. Higashi *et al.* published experimental $P\rho T$ properties, vapour pressures, saturated densities, and critical parameters for HFO-1234ze(Z) [9]. Katsuyuki published experimental vapour pressure and saturated liquid density for HFO-1234ze(E) and HFO-1234ze(Z) [8]. The published experimental data of Higashi *et al.* [9] and Katsuyuki [8] can be used in the study on the refrigeration, heat pump, as well as organic Rankine systems. The above experimental data can be used to develop an equation of state for HFO-1234ze(Z). Akasaka *et al.* [10] and Phan and Lai [11] used the published experimental data to develop the equation of state for HFO-1234ze(Z). The developed equation of state can be used to calculate all thermodynamic properties of HFO-1234ze(Z). The thermodynamic properties of HFO-1234ze(Z) can be used in the study on the refrigeration, heat pump, as well as organic Rankine systems. In practice, the lgP-h diagram is the most common and visual tool. Akasaka *et al.* [10] and Phan and Lai [11] have not published detail thermodynamic properties of HFO-1234ze(Z) and lgP-h diagram for HFO-1234ze(Z). The lgP-h diagram has popularly been used in education and in the design and calculation of heat pump and refrigeration system. Thus, this paper aims to provide the accurate lgP-h diagram and the thermodynamic properties of HFO-1234ze(Z) in both single-phase and two-phase regions.

ISSN 2734-9381
https://doi.org/10.51316/jst.156.etsd.2022.32.1.5
Received: May 8, 2021; accepted: January 28, 2022

2. Equations for the Determination of the Thermodynamic Properties

The thermodynamic properties of fluids can be divided into 2 groups. The first group includes the state properties such as temperature, pressure, and specific volume. The second group includes caloric properties such as enthalpy, internal energy, and entropy. The above properties can be determined from the Helmholtz energy as follows. Pressure is determined from (1):

$$\frac{p(\delta,\tau)}{\rho RT}=1+\delta\left(\frac{F}{RT}\right)_{\delta}^{r} \tag{1}$$

where $\delta=\frac{\rho}{\rho_c}$ is reduced density and $\tau=\frac{T_c}{T}$ is reduced temperature. T_c is critical temperature. ρ_c is critical density. R is the gas constant. F is the Helmholtz energy. The superscript r stands for the real part contribution of dimentionless Helmholtz energy (F/RT).

Entropy is determined from (2):

$$\frac{s(\delta,\tau)}{R}=\tau\left[\left(\frac{F}{RT}\right)_{\tau}^{0}+\left(\frac{F}{RT}\right)_{\tau}^{r}\right]-\left(\frac{F}{RT}\right)^{0}-\left(\frac{F}{RT}\right)^{r} \tag{2}$$

where the superscript 0 stands for the ideal part contribution of dimentionless Helmholtz energy.

Internal energy is determined from (3):

$$\frac{u(\delta,\tau)}{RT}=\tau\left[\left(\frac{F}{RT}\right)_{\tau}^{0}+\left(\frac{F}{RT}\right)_{\tau}^{r}\right] \tag{3}$$

Enthalpy is determined from (4):

$$\frac{h(\delta,\tau)}{RT}=1+\tau\left[\left(\frac{F}{RT}\right)_{\tau}^{0}+\left(\frac{F}{RT}\right)_{\tau}^{r}\right]+\delta\left(\frac{F}{RT}\right)_{\delta}^{r} \tag{4}$$

The ideal part contribution is determined from (5):

$$F^{0}(\rho,T)=h^{0}(T)-RT-Ts^{0}(\rho,T) \tag{5}$$

The real part contribution $F^{r}(\rho,T)$ in this study includes molecular hard-body contribution $F_H(\rho,T)$, attractive dispersion force contribution $F_A(\rho,T)$, and quadrupolar contribution $F_Q(\rho,T)$. The hard-body contribution of Boublik [13] as in (6) is used:

$$\frac{F_H}{RT}=(\alpha^2-1)\ln(1-\xi)+\frac{(\alpha^2+3\alpha)\xi-3\alpha\xi^2}{(1-\xi)^2} \tag{6}$$

where α is the anisotropy factor and ξ is the packing fraction. The packing fraction of Saager [14] as in (7) is used:

$$\xi=\xi_0(\frac{\rho}{\rho_0})\left[a+(1-a)\left(\frac{T}{T_0}\right)^{\gamma}\right]^{-1} \tag{7}$$

The attractive dispersion force contribution of Muller *at el.* [15] as in (8) is used:

$$\frac{F_A}{RT}=\sum\nolimits_i c_i\left(\frac{\rho}{\rho_0}\right)^{m_i}\left(\frac{T}{T_0}\right)^{n_i/2}\alpha^{j_i}\exp\left[-\left(\frac{\rho}{\rho_0}\right)^{l_i}\right] \tag{8}$$

The quadrupolar contribution of Saager [14] as in (9) is used:

$$\frac{F_Q}{RT}=\sum\nolimits_i c_i\left(\frac{\rho}{\rho_0}\right)^{m_i}\left(\frac{T}{1{,}13T_0}\right)^{n_i}(Q^{*2})^{k_i/4}\exp\left[-o_i\left(\frac{\rho}{\rho_0}\right)^{2}\right] \tag{9}$$

Speed of sound is determined from (10):

$$\frac{w^2(\delta,\tau)}{RT}=1+2\delta\left(\frac{F}{RT}\right)_{\delta}^{r}+\delta^2\left(\frac{F}{RT}\right)_{\delta\delta}^{r}-\frac{\left[1+\delta\left(\frac{F}{RT}\right)_{\delta}^{r}-\delta\tau\left(\frac{F}{RT}\right)_{\delta\tau}^{r}\right]^2}{\tau^2\left[\left(\frac{F}{RT}\right)_{\tau\tau}^{0}+\left(\frac{F}{RT}\right)_{\tau\tau}^{r}\right]} \tag{10}$$

Isobaric heat capacity is determined from (11):

$$\frac{c_p(\delta,\tau)}{R}=-\tau^2\left[\left(\frac{F}{RT}\right)_{\tau\tau}^{0}+\left(\frac{F}{RT}\right)_{\tau\tau}^{r}\right]+\frac{\left[1+\delta\left(\frac{F}{RT}\right)_{\delta}^{r}-\delta\tau\left(\frac{F}{RT}\right)_{\delta\tau}^{r}\right]^2}{\left[1+2\delta\left(\frac{F}{RT}\right)_{\delta}^{r}+\delta^2\left(\frac{F}{RT}\right)_{\delta\delta}^{r}\right]} \tag{11}$$

3. Thermodynamic Properties of HFO-1234ze(Z) and Their Accuracy

The above equations (1) to (11) in section 2 can be used to determine all thermodynamic properties of fluid if the molecular characteristics of the fluid are available. The recent study for HFO-1234ze(Z) shows that the characteristic temperature T_0, characteristic density ρ_0, anisotropy factor α, and reduce quarupole moment Q^{*2} for HFO-1234ze(Z) are 413.825496 K, 4.057173 mol/l, 1.44052, and 2.755521, respectively [11]. In this study, the above equations and molecular characteristics are used to determine pressure, enthalpy, internal energy and entropy from a certain given temperature and specific volume.

The calculation tool for the determination of the thermodynamic properties of HFO-1234ze(Z) is not available for many readers and the available thermodynamic properties for HFO-1234ze(Z) are not available for the full fluid region even though the equation of state for HFO-1234ze(Z) have been published by Akasaka *et al.* [10] and Phan and Lai [11]. Thus, for the convenience of the readers, all the important thermodynamic properties for the full fluid region are presented in this study.

Fig. 1 shows the lgP-h diagram of HFO-1234ze(Z). The reference states for enthalpy and entropy are 200 kJ/kg and 1.0 kJ/(kg·K) for the

saturated liquid at 273.15 K (designated as IIR). This diagram includes pressure, enthalpy, temperature, entropy and specific volume. The internal energy can be calculated from the given enthalpy, specific volume and pressure. Thus, all the important state properties and caloric properties can be determined from the lgP-h diagram.

For scientists, engineers, technicians and anyone trying to get the detail data of HFO-1234ze(Z), all the important thermodynamic properties of HFO-1234ze(Z) are also presented in tables. Table 1 shows the saturated thermodynamic properties of HFO-1234ze(Z) within the interest temperature range from -30 ºC to 150 ºC. Table 2 shows the thermodynamic properties of HFO-1234ze(Z) cover the temperature range from -30 ºC to 260 °C, the pressure ranges from 0.06 up to 4 MPa in the single-phase region.

In order to evaluate the accuracy of the thermodynamic properties of HFO-1234ze(Z) in Fig.1 and Tables 1 and Table 2, the available experimental data published by Fedele *et al*. [16], Katsuyuki [8], Fedele *et al*. [12], and Higashi [9] were used. The average absolute deviation (AAD) between calculated vapour pressure and all experimental vapour pressure published by Fedele *et al*. [16] are only 0.43%. The AAD between calculated saturated liquid density and those from Katsuyuki [8] are 0.43%. The relative deviations between calculated gas density ($\rho_{g,cal}$) and experimental gas density ($\rho_{g,exp}$) of Fedele *et al.* [12] at different temperature varies from 0.1% to 3.54%, the AAD of 1.6%. The relative deviations between the calculated liquid density ($\rho_{l,cal}$) and experimental liquid density ($\rho_{l,exp}$) of Higashi [9] varies from -0.36% to 0.95%, the AAD for 312 data points of 0.68%. The detailed results of the above evaluations are presented in [11].

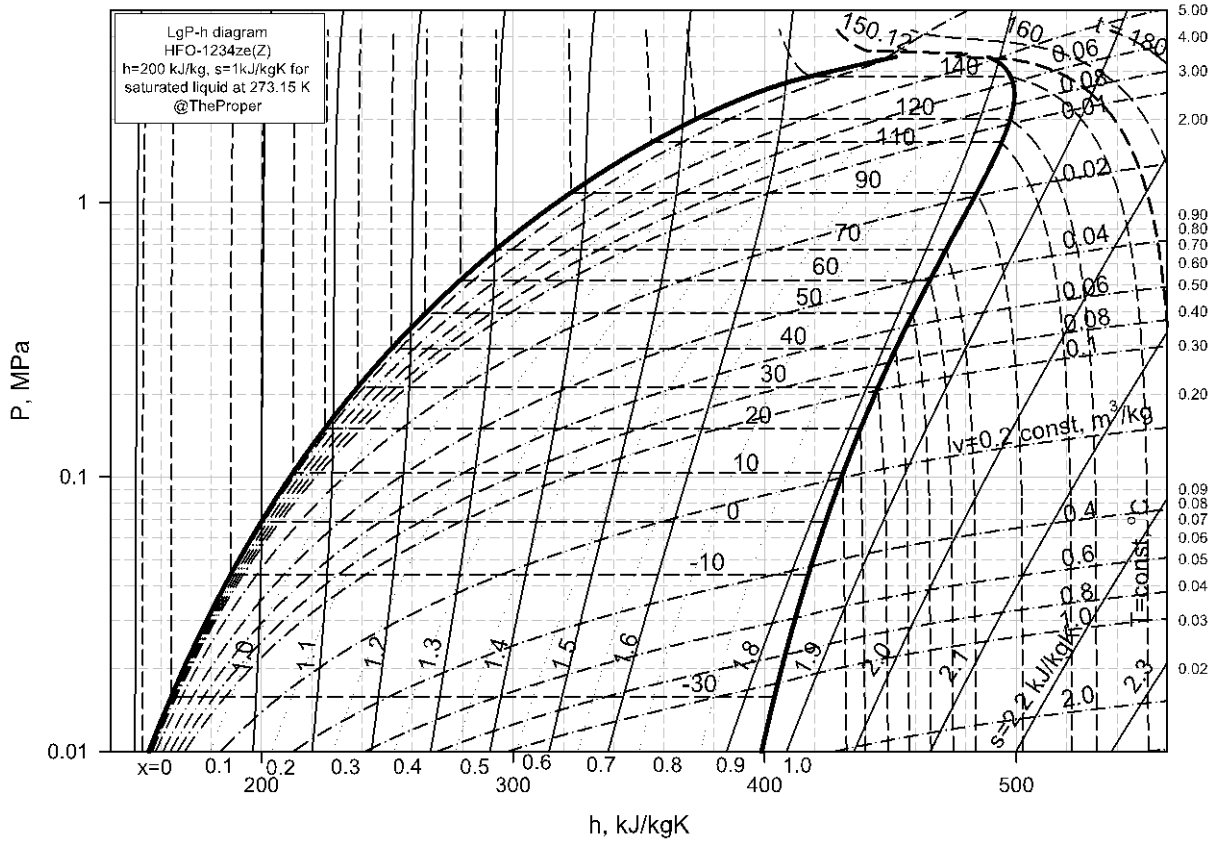

Fig. 1. LgP-h of HFO-1234ze(Z).

Table 1. Saturated thermodynamic properties of HFO-1234ze(Z).

T, ^{o}C	P MPa	ρ_l, kg m^{-3}	ρ_g, kg m^{-3}	h_l, kJ kg^{-1}	h_g, kJ kg^{-1}	s_l, kJ kg^{-1} K^{-1}	s_g, kJ kg^{-1} K^{-1}	w_l, m s^{-1}	w_g, m s^{-1}
-30	0.016	1350	0.90	164.1	403.9	0.861	1.847	810	140
-20	0.027	1327	1.49	175.8	410.5	0.908	1.835	779	142
-15	0.035	1315	1.88	181.8	413.9	0.931	1.831	764	143
-10	0.044	1303	2.34	187.8	417.3	0.954	1.827	749	144
-5	0.055	1291	2.90	193.8	420.8	0.977	1.824	733	144
0	0.069	1279	3.55	200.0	424.2	1.000	1.821	718	145
5	0.085	1266	4.31	206.2	427.7	1.023	1.819	703	146
10	0.103	1254	5.20	212.5	431.2	1.045	1.817	688	146
15	0.125	1241	6.22	218.8	434.6	1.067	1.816	672	147
20	0.150	1229	7.40	225.3	438.1	1.089	1.815	657	147
25	0.179	1216	8.74	231.7	441.6	1.111	1.815	641	147
30	0.212	1203	10.26	238.3	445.1	1.132	1.815	625	148
35	0.250	1189	11.98	244.9	448.6	1.154	1.815	609	148
40	0.292	1176	13.93	251.6	452.0	1.175	1.816	592	148
45	0.340	1162	16.11	258.3	455.5	1.197	1.816	576	147
50	0.394	1149	18.56	265.1	458.9	1.218	1.817	559	147
55	0.454	1134	21.29	272.0	462.3	1.239	1.819	541	147
60	0.520	1120	24.34	279.0	465.6	1.260	1.820	523	146
65	0.593	1105	27.75	286.1	468.9	1.281	1.821	505	145
70	0.674	1090	31.53	293.2	472.1	1.301	1.823	486	144
75	0.763	1075	35.75	300.5	475.3	1.322	1.824	467	143
80	0.860	1058	40.44	307.8	478.4	1.343	1.826	447	142
85	0.966	1042	45.66	315.3	481.4	1.364	1.827	426	140
90	1.081	1024	51.48	322.9	484.2	1.384	1.829	404	138
95	1.207	1006	57.99	330.7	487.0	1.405	1.830	382	136
100	1.343	986	65.28	338.6	489.5	1.426	1.831	359	134
105	1.490	965	73.48	346.7	491.9	1.447	1.831	334	132
110	1.648	943	82.76	355.0	494.1	1.469	1.832	308	129
115	1.819	918	93.35	363.7	496.0	1.491	1.832	281	126
120	2.003	890	105.53	372.6	497.6	1.513	1.831	251	122
130	2.410	819	136.62	392.3	499.2	1.561	1.827	184	114
140	2.870	681	182.89	418.1	497.7	1.623	1.816	105	104
150	3.373	481	268.01	451.9	488.9	1.702	1.789	86	93

Table 2. Thermodynamic properties of HFO-1234ze(Z) in the single-phase state.
(h, kJ kg^{-1}; s, kJ kg^{-1} K^{-1}; v, m^3 kg^{-1})

T, °C	P, MPa	0.06	0.08	0.1	0.2	0.4	0.6	0.8	1	2	4
	h	164.17	164.18	164.19	164.23	164.32	164.40	164.49	164.58	165.01	165.89
-30	s	0.861	0.861	0.861	0.861	0.861	0.860	0.860	0.860	0.859	0.856
	v	7.41E-04	7.41E-04	7.41E-04	7.40E-04	7.40E-04	7.40E-04	7.40E-04	7.40E-04	7.38E-04	7.36E-04
	h	175.82	175.83	175.84	175.88	175.96	176.05	176.13	176.21	176.63	177.47
-20	s	0.908	0.908	0.908	0.908	0.908	0.907	0.907	0.907	0.906	0.903
	v	7.54E-04	7.54E-04	7.54E-04	7.53E-04	7.53E-04	7.53E-04	7.53E-04	7.52E-04	7.51E-04	7.49E-04
	h	424.47	200.00	200.01	200.05	200.12	200.20	200.27	200.35	200.72	201.49
0	s	1.831	1.000	1.000	1.000	1.000	0.999	0.999	0.999	0.997	0.994
	v	3.24E-01	7.82E-04	7.82E-04	7.82E-04	7.82E-04	7.81E-04	7.81E-04	7.81E-04	7.79E-04	7.76E-04
	h	432.34	431.80	431.25	212.53	212.60	212.67	212.74	212.81	213.16	213.88
10	s	1.860	1.837	1.820	1.045	1.044	1.044	1.044	1.043	1.042	1.039
	v	3.37E-01	2.51E-01	1.99E-01	7.97E-04	7.97E-04	7.97E-04	7.96E-04	7.96E-04	7.94E-04	7.90E-04
	h	440.41	439.93	439.43	225.27	225.33	225.39	225.46	225.52	225.84	226.51
20	s	1.888	1.866	1.848	1.089	1.089	1.088	1.088	1.088	1.086	1.083
	v	3.49E-01	2.60E-01	2.07E-01	8.14E-04	8.13E-04	8.13E-04	8.13E-04	8.12E-04	8.10E-04	8.06E-04
	h	448.69	448.25	447.80	445.42	238.32	238.38	238.43	238.49	238.78	239.38
30	s	1.916	1.894	1.876	1.820	1.132	1.132	1.131	1.131	1.129	1.126
	v	3.62E-01	2.70E-01	2.15E-01	1.04E-01	8.31E-04	8.31E-04	8.30E-04	8.30E-04	8.27E-04	8.22E-04
	h	457.17	456.77	456.36	454.21	251.58	251.62	251.67	251.72	251.96	252.49
40	s	1.943	1.921	1.904	1.848	1.175	1.175	1.174	1.174	1.172	1.168
	v	3.75E-01	2.80E-01	2.22E-01	1.08E-01	8.50E-04	8.49E-04	8.49E-04	8.48E-04	8.45E-04	8.40E-04
	h	465.85	465.47	465.10	463.14	265.12	265.16	265.19	265.23	265.42	265.85
50	s	1.970	1.949	1.931	1.877	1.218	1.217	1.217	1.216	1.214	1.210
	v	3.87E-01	2.89E-01	2.30E-01	1.12E-01	8.71E-04	8.70E-04	8.69E-04	8.69E-04	8.65E-04	8.59E-04
	h	474.72	474.38	474.03	472.24	468.29	279.01	279.03	279.05	279.17	279.48
60	s	1.997	1.976	1.959	1.904	1.845	1.260	1.259	1.259	1.256	1.252
	v	4.00E-01	2.99E-01	2.38E-01	1.16E-01	5.53E-02	8.92E-04	8.92E-04	8.91E-04	8.87E-04	8.79E-04
	h	493.03	492.74	492.44	490.92	487.64	483.97	479.76	307.82	307.71	307.64
80	s	2.051	2.029	2.012	1.959	1.901	1.864	1.834	1.342	1.339	1.334
	v	4.25E-01	3.18E-01	2.53E-01	1.24E-01	5.98E-02	3.81E-02	2.71E-02	9.44E-04	9.38E-04	9.26E-04
	h	512.09	511.83	511.58	510.26	507.47	504.43	501.09	497.35	338.19	337.35
100	s	2.103	2.082	2.065	2.012	1.956	1.920	1.893	1.869	1.423	1.416
	v	4.50E-01	3.36E-01	2.68E-01	1.32E-01	6.40E-02	4.12E-02	2.97E-02	2.27E-02	1.01E-03	9.86E-04
	h	531.85	531.63	531.40	530.24	527.83	525.25	522.48	519.48	497.67	369.47
120	s	2.155	2.133	2.117	2.064	2.009	1.975	1.949	1.927	1.831	1.500
	v	4.74E-01	3.55E-01	2.83E-01	1.40E-01	6.82E-02	4.42E-02	3.22E-02	2.49E-02	9.50E-03	1.07E-03
	h	552.29	552.09	551.89	550.86	548.74	546.50	544.15	541.65	525.88	406.83
140	s	2.205	2.184	2.168	2.115	2.061	2.028	2.002	1.982	1.901	1.592
	v	4.99E-01	3.74E-01	2.98E-01	1.48E-01	7.23E-02	4.71E-02	3.45E-02	2.69E-02	1.13E-02	1.24E-03
	h	573.40	573.20	573.00	572.10	570.20	568.20	566.20	564.00	551.50	470.80
160	s	2.255	2.234	2.217	2.165	2.112	2.079	2.054	2.035	1.962	1.743
	v	5.24E-01	3.92E-01	3.13E-01	1.55E-01	7.63E-02	4.99E-02	3.67E-02	2.88E-02	1.27E-02	2.25E-03
	h	595.10	594.90	594.70	593.90	592.20	590.50	588.70	586.80	576.30	543.70
180	s	2.304	2.283	2.266	2.215	2.161	2.129	2.105	2.086	2.018	1.908
	v	5.48E-01	4.11E-01	3.28E-01	1.63E-01	8.02E-02	5.26E-02	3.88E-02	3.06E-02	1.39E-02	4.96E-03
	h	617.30	617.20	617.00	616.30	614.70	613.20	611.60	609.90	600.80	576.90
200	s	2.352	2.331	2.315	2.263	2.210	2.178	2.155	2.136	2.071	1.980
	v	5.73E-01	4.29E-01	3.43E-01	1.70E-01	8.41E-02	5.53E-02	4.09E-02	3.23E-02	1.49E-02	6.00E-03
	h	640.10	640.00	639.90	639.20	637.80	636.40	634.90	633.40	625.50	606.20

Table 2. *(Cont.)*

T, °C	P, MPa	0.06	0.08	0.1	0.2	0.4	0.6	0.8	1	2	4
220	s	2.400	2.378	2.362	2.310	2.258	2.226	2.203	2.184	2.122	2.041
	v	5.97E-01	4.48E-01	3.58E-01	1.78E-01	8.80E-02	5.80E-02	4.30E-02	3.40E-02	1.59E-02	6.79E-03
	h	663.50	663.30	663.20	662.60	661.30	660.00	658.70	657.30	650.30	634.00
240	s	2.446	2.425	2.408	2.357	2.304	2.273	2.250	2.232	2.171	2.096
	v	6.22E-01	4.66E-01	3.72E-01	1.85E-01	9.18E-02	6.06E-02	4.50E-02	3.57E-02	1.69E-02	7.47E-03
	h	687.30	687.20	687.10	686.50	685.30	684.10	682.90	681.70	675.30	661.20
260	s	2.491	2.470	2.454	2.403	2.350	2.319	2.296	2.279	2.219	2.148
	v	6.46E-01	4.84E-01	3.87E-01	1.93E-01	9.56E-02	6.32E-02	4.70E-02	3.73E-02	1.78E-02	8.08E-03

To enhance reliability of the obtained research, some other thermodynamic properties of HFO-1234ze(Z) such as the ideal gas heat capacity and the speed of sound are additionally evaluated with available experimental data. The calculated speed-of-sound data is compared to published experimental data from Lago *et al.* [17] and Lozano *et al.* [18]. Lago *et al.* [17] published 38 experimental speed-of-sound data points in the compressed liquid phase of R-1234ze(Z)) for temperature ranging from 273.15 K to 333.15 K and pressures up to 25 MPa. The measurements were taken by employing the double pulse-echo technique. The expanded uncertainty of the measured data was reported less than 0.05% at the 95% confidence level over the entire thermodynamic space. Lozano *et al.* [18] published 94 experimental gaseous speed-of-sound data points for temperature ranging from 307 K to 420 K and pressures up to 1.8 MPa using a quasi-spherical acoustic resonato. The relative accuracy of their determinations of the speed of sound *w(p,T)* of HFO-1234ze(Z) was said to be about ± 0.02%.

All the relative differences between calculated data for speed of sound and experimental data were shown in Fig. 2 and Fig. 3. Fig. 2 shows deviations between the calculated speed-of-sound data in [11] and experimental data of Lago *et al.* [17]. Relative deviations between calculated value and experimental data for 38 data points range from -5.53% to 4.86%. The AAD for 38 data points are 2.2%, while the relative deviations between experimental results obtained in *Lago et al.* [17] with respect to those estimated using Akasaka's EoS [10] vary from being 1.3% to 7.0% greater, with a mean of 4.1%. This proves the reliability of the recent study [11] for HFO-1234ze(Z).

Deviations between the calculated speed-of-sound data in [11] and those from Lozano *et al.* [18] are shown in Fig. 3. Relative deviations between calculated value and experimental data for 94 data points range from -2.7% to 0.01%. Fig. 3 shows that most of relative deviations are negative differences and deviations increase with the increase of pressure. The deviations clearly indicate that the present study is a good predictive equation of state because the AAD for speed-of-sound data in gas phase is about 0.98% for the nine isotherms, between 307 K and 420 K. It shows reasonable consistency of obtained data in comparing with all available experimental speed-of-sound data.

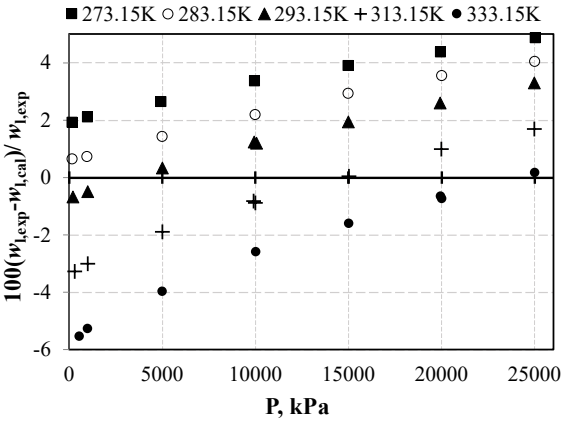

Fig. 2. Deviation of compressed liquid speed-of-sound data ($w_{g,cal}$) from [11] and experimental data ($w_{g,exp}$) of Lago *et al.* [17].

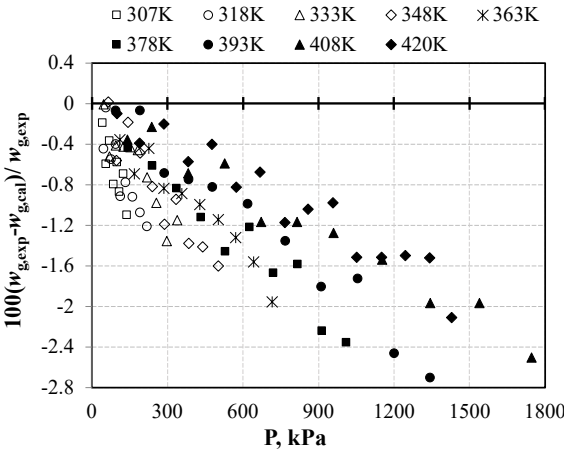

Fig. 3. Deviation of gaseous speed-of-sound data ($w_{g,cal}$) from [11] and experimental data ($w_{g,exp}$) of Lozano *et al.* [18].

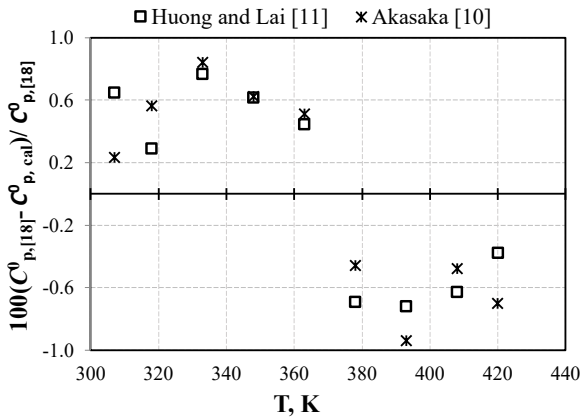

Fig. 4. Deviation of the ideal gas heat capacities determined in [11] and those of Akasaka *et al.* [10] and pulished data of Lozano *et al.* [18]

From the experimental speed-of-sound data, the ideal gas heat capacities at temperatures between 307 K and 420 K were deduced in Lozano *et al.* [18]. The accuracy of the determination of the ideal gas heat capacity ratio γ^0 (T) was reported to be approximately ± 0.25%. Fig. 4 compares our determinations of C^0_p and the predictions of Akasaka *et al.* [10] with published data in [18]. Relative deviations between the calculated data in [11] and published data of [18] range from -0.72% to 0.76% and the AAD is 0.57%, whereas those of Akasaka [10] varies from -0.94% to 0.84% and the AAD is 0.59%. These findings are consistent with the recent published data and provide acceptably accurate results.

To the best of the authors' knowledge, there is no other experimental thermodynamic data of HFO-1234ze(Z) at the moment, so further evaluation of the rest of data accuracies are impossible until there are new publicly available databases.

4. Conclusion

Thermodynamic properties for HFO-1234ze(Z) in both the single-phase region and two-phase region were determined. These data then were plotted in the lgP-h diagram and presented in table for saturated properties and the table for liquid and vapour phase region. The published figure and tables can be used in the design and evaluation of the heat pump, of the air-conditioning system, of the organic Rankine system using HFO-1234ze(Z) as working fluid and refrigerant. The accuracy of the calculated and published thermodynamic properties of HFO-1234ze(Z) was evaluated by comparison with available experimental data. The AAD between calculated vapour pressure data and experimental data of Fedele [16] were 0.43%. The AAD between calculated saturated liquid density data and experimental data of Katsuyuki [8] were 0.43%. In the prediction of the thermodynamic properties, AAD between calculated liquid density data and experimental data were 0.68% and AAD between calculated gas density data and experimental data were 1.6%. The AAD between calculated liquid speed-of-sound data and experimental data were 2.2% and the AAD between calculated gaseous speed-of-sound data and experimental data were 0.98%. The AAD between calculated ideal gas heat capacity data and published data were 0.57%.

Acknowledgements

This research is funded by the Vietnam National Foundation for Science and Technology Development (NAFOSTED) under grant number 107.03-2016.10. The author gratefully acknowledges financial support from the NAFOSTED.

Reference

[1] United Nations Environment Program (UNEP), Montreal Protocol on Substances that Deplete the Ozone Layer, Final Act, United Nations, New York, 1997.

[2] Kyoto Protocol, Report of the Conference of the Parties, United Nations Framework Convention on Climate Change (UNFCCC), 1997.

[3] UNEP Ozone Secretariat, TEAP 2010 progress report volume 1 assessment of HCFCS and environmentally sound alternatives, 2010.

[4] Environmental Protection Agency (EPA), Protection of Stratospheric Ozone: Proposed New Listings of Substitutes, US Environmental Protection Agency, 2016.

[5] The European parliament and the council, Regulation (EU) no 517/2014 of the European parliament and of the council, OJ L, vol. 150, 2014, pp. 195–230.

[6] Japan Ministry of the Environment, Revised F-Gas Law in Japan, 2015. Available: http://www.env.go.jp/earth/ozone/hiyasu-waza/eng/revised_f-gas_law_in_japan.html.

[7] M.O.K McLinden, F.A. Steven Brown, J. Domanski, Piotr A, A thermodynamic analysis of refrigerants: Possibilities and tradeoffs for Low-GWP refrigerants, Int J Refrig, vol. 38, pp. 80–92, 2014, https://doi.org/10.1016/j.ijrefrig.2013.09.032.

[8] T. Katsuyuki, Measurements of Vapor Pressure and Saturated Liquid Density for HFO–1234ze(E) and HFO–1234ze(Z), J. Chem. Eng. Data, vol. 61, pp. 1645–1648, 2016 https://doi.org/10.1021/acs.jced.5b01039.

[9] Y. Higashi, S. Hayasaka, C. Shirai, R. Akasaka, Measurements of PρT properties, vapor pressures, saturated densities, and critical parameters for R 1234ze(Z) and R 245fa, Int J Refrig, vol. 52, pp. 100–108, 2015 https://doi.org/10.1016/j.ijrefrig.2014.12.007.

[10] R. Akasaka, Y. Higashi, A. Miyara, S. Koyama, A fundamental equation of state for cis-1,3,3,3-tetrafluoropropene (R-1234ze(Z)), Int J Refrig, vol. 44, pp. 168–176, 2014 https://doi.org/10.1016/j.ijrefrig.2013.12.018.

[11] T.T.H. Phan, N.A. Lai, Backone equation of state for cis-1,3,3,3-tetrafluoropropene (HFO-1234ze(Z)), VAJC, vol. 40, pp. 387–395, 2018 https://doi.org/https://doi.org/10.15625/0866-7136/13207.

[12] L. Fedele, J.S. Brown, G. Di Nicola, S. Bobbo, M. Scattolini, Measurements and correlations of cis-1,3,3,3-Tetrafluoroprop-1-ene (R1234ze(Z)) subcooled liquid density and vapor-phase PvT, Int. J. Thermophys., vol. 35, pp. 1415–1434, 2014 https://doi.org/10.1007/s10765-014-1730-1.

[13] T. Boublík, Hard convex body equation of state, J. Chem. Phys., vol. 63, pp 4084, 1975 https://doi.org/10.1063/1.431882.

[14] B. Saager, R. Hennenberg, J. Fischer, Construction and application of physically based equations of state, Fluid Phase Equilib, vol. 72, pp. 41–66, 1992, https://doi.org/10.1016/0378-3812(92)85018-4.

[15] J.W. Andreas Miiller Johann Fischer, Backone family of equations of state: 1. Nonpolar and polar pure fluids, AIChE Journal, vol. 42, pp. 1116–1126, 1996, https://doi.org/10.1002/aic.690420423.

[16] L. Fedele, G. Di Nicola, J.S. Brown, S. Bobbo, C. Zilio, Measurements and correlations of cis-1,3,3,3-Tetrafluoroprop-1-ene (R1234ze(Z)) saturation pressure, Int. J. Thermophys., vol. 35, pp 1–12, 2014, https://doi.org/10.1007/s10765-013-1553-5.

[17] S. Lago, P.A. Giuliano Albo, J. Steven Brown., Compressed liquid speed of sound measurements of cis-1,3,3,3-tetrafluoroprop-1-ene (R1234ze(Z)), Int. J. Refrig., vol. 65, pp. 55-59, 2016 https://doi.org/10.1016/j.ijrefrig.2016.02.003.

[18] D. Lozano-Martín, D.M. Ripa and R.M. Gavioso, Speed of sound in gaseous cis-1,3,3,3-tetrafluoropropene (R1234ze(Z)) between 307 K and 420 K, Int J Refrig., vol. 100, pp. 37-47, 2019 https://doi.org/10.1016/j.ijrefrig.2019.01.021.